

## Article

# Tribocorrosion Performance of WC-12Co HVOF-Sprayed Coatings Reinforced with Carbon Nanotubes

Mariana Henriette Staia <sup>1,2,3</sup>, Alberto Mejias <sup>2,4,\*</sup>, Stephania Kossman <sup>2</sup>  and Eli Saul Puchi-Cabrera <sup>1,3</sup>

<sup>1</sup> School of Metallurgical Engineering and Materials Science, Faculty of Engineering, Universidad Central de Venezuela, Los Chaguaramos, Caracas 1050, Venezuela

<sup>2</sup> Arts et Métiers Institute of Technology, Laboratory of Mechanics, Surface, Materials and Processes (MSMP), HESAM Université, 59800 Lille, France

<sup>3</sup> Venezuelan National Academy for Engineering and Habitat, Palacio de las Academias, Caracas 1012, Venezuela

<sup>4</sup> Junia, Department of Smart Systems & Energies, 59000 Lille, France

\* Correspondence: alberto.mejias@junia.com

**Abstract:** WC-12Co HVOF-sprayed coatings (~400 μm in thickness) reinforced with multiwalled carbon nanotubes (MWCNTs), were deposited on a steel substrate. The aim of this work is to provide and analyze data from HVOF WC-12Co sprayed coatings, concerning the influence of the addition of MWCNTs on their tribocorrosion performance, in a 3.5% NaCl electrolyte. Electrochemical data (current density and corrosion potential from potentiodynamic polarization curves) and wear data (coefficients of friction, coating volume losses and wear constants) are reported for the coatings, with and without the addition of MWCNTs (labeled WC<sub>CNT</sub> and WC<sub>AS-RECEIVED</sub>, respectively), considering the synergistic effects of wear and corrosion coupling. Scanning electron microscopy (SEM) and profilometry are used to explain both the wear and corrosion mechanisms that account for each coating's performance in this environment. During the tribocorrosion tests, similar wear constants, of the order of approximately 10<sup>-12</sup> m<sup>3</sup>/Nm, were found for all samples, with an increase of ~20% due to the MWCNTs presence. However, for the coatings reinforced with MWCNTs, a remarkable increase in *i*<sub>corr</sub>, representing almost 3 times the *i*<sub>corr</sub> of the WC<sub>AS-RECEIVED</sub> coating, was determined. The above results illustrate the complex mechanisms that occur when these coatings are tested under tribocorrosion conditions, which give rise to concurrent interacting phenomena, involving both electrochemical and mechanical responses.

**Keywords:** tribocorrosion performance; wear; WC-Co coating; carbon nanotubes; HVOF; hard chrome replacement; corrosion mechanisms



**Citation:** Staia, M.H.; Mejias, A.; Kossman, S.; Puchi-Cabrera, E.S. Tribocorrosion Performance of WC-12Co HVOF-Sprayed Coatings Reinforced with Carbon Nanotubes. *Crystals* **2023**, *13*, 457. <https://doi.org/10.3390/cryst13030457>

Academic Editors:

Daniela-Lucia Chicet and Ștefan-Lucian Toma

Received: 13 February 2023

Revised: 28 February 2023

Accepted: 3 March 2023

Published: 6 March 2023



**Copyright:** © 2023 by the authors. Licensee MDPI, Basel, Switzerland. This article is an open access article distributed under the terms and conditions of the Creative Commons Attribution (CC BY) license (<https://creativecommons.org/licenses/by/4.0/>).

## 1. Introduction

Research on alternatives to hard chromium plating (a well-known surface engineering process, which gives rise to an increase in corrosion and wear resistance of the coated substrate) has been a high priority in recent years, due to the toxicity related with the use of hexavalent chromium and the environmental impact of its production [1–3]. Thermal spraying processes have been extensively studied, with the aim of finding a replacement for this type of coating. One of these processes is high velocity oxy-fuel (HVOF), a common combustion-spraying method, using oxygen as oxidant, and widely employed in different industries [2,4], where process parameters play an essential role on the coating properties and performance (porosity, microhardness, tribological behavior, etc.), as has recently been documented [5].

Thermal spray coating deposition ranges from pure metals (such as copper, nickel, tungsten, etc.) and alloy coatings (for instance Hastalloys, Monel, stainless steel, etc.), to cermet powders (WC-Co, Cr<sub>3</sub>C<sub>2</sub>-NiCr, etc.), as well as other ceramic materials (for example, ZrO<sub>2</sub>, Al<sub>2</sub>O<sub>3</sub>, YSZ: yttria-stabilized zirconia) [6,7]. In particular, the thermal sprayed

coatings based on WC–Co provide high wear resistance for a wide range of industrial applications, which include aircraft, as well as manufacturing and mining industries. Different research works have been conducted recently to study the wear and corrosion performance of WC–Co drilling tools [7–9], to better understand the failure mechanisms of these components under severe working conditions (frictional contact in aqueous environments).

Concerning feedstock materials suitable for thermal spraying processes, MWCNTs reinforced metal matrix composites have been an explored alternative, regarding their mechanical behavior. Since their discovery, MWCNTs have been considered to be one of the major components for the reinforcement of metal matrix composites, that could bring about considerable improvements in the strengthening mechanisms and mechanical properties of these materials. Nevertheless, the incorporation of MWCNTs into cermet powders aimed at HVOF coating deposition has been considered with some reserve. Critical issues concerning the use of MWCNTs as reinforcing elements have been reviewed in detail by Bakshi et al. [10]. These authors addressed several problems of these materials, concerning processing techniques and dispersion, as well as structural and chemical stability in several metal matrix composites. In addition, these authors have discussed their strengthening mechanisms and mechanical properties, which are of fundamental importance for their potential application in the HVOF coating deposition industry.

In the past few years, important work has been conducted aimed at characterizing the wear and corrosion resistance of different coatings reinforced with MWCNTs [11–13]. Deesom et al. [11] reported the development of a NiCr/MWCNTs composite feedstock powder synthesized by means of a chemical vapor deposition (CVD) process and ball milling, without the use of a catalyst. Wear tests were performed by means of a pin-on-disc tribometer, and potentiodynamic polarization experiments were carried out to evaluate the corrosion performance. These authors demonstrated that MWCNTs-reinforced NiCr composite coatings, HVOF-sprayed onto mild steel substrates, provided higher hardness and wear resistance, as well as an improved corrosion resistance, in comparison to the unreinforced NiCr coating.

Later, Dong et al. [12], on the other hand, have characterized the effect of MWCNTs concentration on the microstructure and friction behavior of nickel-graphene oxide composite coatings deposited on magnesium alloy substrates, by means of an integrative method, involving electrophoresis and electrodeposition. It was demonstrated that these composite coatings exhibited a lower coefficient of friction, smaller wear loss, and better wear resistance up to a limited MWCNTs concentration of 0.4 g/L. However, as soon as this concentration was exceeded, defects, such as voids accompanied with cracks in the composite coating appeared, which gave rise to a reduction in its mechanical and tribological performance.

More recently, Ujah et al. [13] showed that MWCNTs-reinforced aluminum alloy, produced by means of spark plasma sintering, exhibited a refined microstructure, high mechanical strength, and improved corrosion performance, as compared with the pure metal matrix sample, which could be attributed to the homogeneous dispersion of the MWCNTs in the matrix. Although the corrosion behavior in the research cited above was evaluated by potentiodynamic polarization curves, other corrosion techniques, such as electrochemical impedance spectroscopy (EIS), could be employed to evaluate the performance of the metal matrix composite's passive layer [14,15].

In spite of the important work that has been conducted in the past few years, to investigate the effect of MWCNTs on the mechanical properties, as well as separate wear and corrosion resistance, of metal matrix composites, the effect of the wear-corrosion coupling performance has been addressed to a lesser extent. An example is the evaluation of the tribocorrosion behavior of MWCNTs-reinforced coatings, which involves the consideration of the synergistic effect of the wear and corrosion coupling on the performance of such materials. Particularly, very limited information has been reported in the scientific literature in relation to the microstructure, mechanical properties, wear, and tribocorrosion performance of MWCNTs-reinforced WC–Co coatings sprayed by means of HVOF techniques.

The earliest report on the effects of the addition of MWCNTs on the microstructure, hardness, and wear resistance of a WC-12Co HVOF-sprayed coating is that of Rodríguez et al. [16], who performed wear tests by employing a dry sand rubber wheel technique. Subsequent work, conducted by Santana et al. [17], allowed the characterization of the wear performance of the same coatings by means of a ball-on-disc tribometer. More recently, Staia et al. [18] have assessed different mechanical properties of both unreinforced and reinforced WC-Co coated systems, including elastic moduli, apparent yield stress, and fracture toughness, to explain the improved tribological performance of the reinforced coatings.

Based on the research works cited above [16–18], the present investigation has been conducted in order to evaluate the tribocorrosion performance of a WC-12Co coating reinforced with MWCNTs, deposited by means of an HVOF process, and to compare it with that of the unreinforced coating, deposited under similar process conditions, with analogous feedstock powders, in terms of phase composition and porosity. To the best of our knowledge, the tribocorrosion performance of this type of reinforced metal matrix composites has not been addressed in the current literature. For this purpose, an innovative, in-house-designed and manufactured tribocorrosion cell (TC), conceived for this kind of sample, was employed. Thus, the computation of the wear volumes and wear constants of the different coatings, tested in a 3.5% NaCl solution, allowed an understanding of the role played by the reinforcement of MWCNTs on the tribocorrosion performance of these cermet materials.

## 2. Materials and Methods

### 2.1. WC-Co Powders

Conventional spray dried agglomerate WC-12Co (identified from here on as P-WC<sub>AS-RECEIVED</sub>), obtained from Polymet (West Chester, OH, USA), with a nominal particle size distribution between 15 and 45 µm, was used as feedstock to produce the coatings. As indicated above, MWCNTs were used as a reinforcing material. These were produced by a CVD method and supplied by Shenzhen Nanotech Port Co. (Shenzhen, China), with the following characteristics: purity > 95%,  $\varnothing_{\text{ext}} \sim 20\text{--}40$  nm, and length  $\sim 5\text{--}15$  µm.

The P-WC<sub>AS-RECEIVED</sub> and the MWCNTs (0.35 wt.%) were previously ultrasonically dispersed in ethanol (purity 99%) for 2 h. Subsequently, these were blended in a jar milling (coated inside with thermally sprayed WC-12Co) at 60 rpm, using WC balls with a diameter of 0.6 mm. Milling was also conducted in ethanol for 36 h, the time required to obtain the optimal powder (identified as P-WC<sub>CNT</sub>), according to [17]. The P-WC<sub>AS-RECEIVED</sub> feedstock was also milled for 36 h (labeled as P-WC<sub>CONV</sub>), to obtain a powder with a similar particle distribution as the mixture P-WC<sub>CNT</sub>. The blending process was also carried out in a jar mill, with an ethanol solution, for 36 h (best dispersion time, according to [16]), at 60 rpm, using similar WC balls. The details of the blending process, as well as the results of the particle size distribution analysis before and after the dispersion process, were described in a previous work [16]. The morphological and chemical analysis was carried out by using a field emission scanning microscope equipped with an energy dispersive X-ray spectrometer (EDS) and micro-Raman analysis, and no detection of any oxide at the interface between the coating and MWCNTs was found.

### 2.2. HVOF Process

The powders were deposited on SAE 1020 steel substrates using a HVOF thermal spray process, with a JP-5000 gun, according to the parameters indicated in Table 1. The oxygen/kerosene flow ratio employed was  $\sim 3$ .

After deposition, the HVOF-sprayed coated samples were polished by using standard metallographic techniques, until a roughness parameter  $R_a \sim 0.05\text{--}0.07$  µm was obtained.

**Table 1.** HVOF thermal spray parameters and coating morphology.

Sample	Stand-off Distance (mm)	Fuel Flow Rate (l/h)	Oxygen Flow Rate (l/h)	Powder Feed Rate (g/min)	Coating Thickness $t$ ( $\mu\text{m}$ )	Coating Porosity (%)
WC <sub>AS-RECEIVED</sub>	300	25.8	80	100	453 $\pm$ 5	3.3 $\pm$ 0.4
WC <sub>CONV</sub>					540 $\pm$ 5	2.3 $\pm$ 0.3
WC <sub>CNT</sub>					520 $\pm$ 6	1.3 $\pm$ 0.3

### 2.3. Experimental Procedure

#### 2.3.1. Wear Tests in Aqueous Solution

Wear tests were conducted in a NaCl electrolyte at room temperature (22 °C), employing a standard ball-on-disc tribometer (TRIBOTester, Tribotechnic, Clichy, France), with an alumina ball (grade 25, according to ISO 3290-2) of 10 mm diameter as counter-body, which allowed the assessment of the coatings' wear performance under corrosive conditions. The tests were carried out with a normal load of 10 N, corresponding to a contact pressure of ~1300 MPa, and a maximum shear stress of ~390 MPa at 30  $\mu\text{m}$  from the top surface, according to the computations conducted by means of Hertz equations. A sliding speed of 12.6 mm/s (60 rpm) was employed, and the sliding distance was 35 m (equivalent to ~2800 cycles). The nominal wear radius ( $r$ ) was ~2 mm. The contact interval time was 1000 ms.

#### 2.3.2. Tribocorrosion Test Setup

Tribocorrosion measurements were carried out using a typical three-electrode configuration: The WC-12Co coatings as working electrodes (WE), with an appropriately isolated exposed area to the corrosive medium of 1.76 cm<sup>2</sup>, an Ag/AgCl/KCl<sub>sat</sub> (+197 mV/SHE) as reference electrode (RE), and a platinum coil as counter electrode. The tribocorrosion tests were performed using an innovative in-house-designed and built tribocorrosion cell (TC), especially conceived for this kind of sample. The cell was manufactured by 3D printing and is shown in Figure 1. Due to the advantageous characteristics of the cell, it is considered that the uncertainties related to sample mounting are considerably reduced and therefore, the tests reproducibility will not be compromised regarding the setup configuration and the WE exposed area.

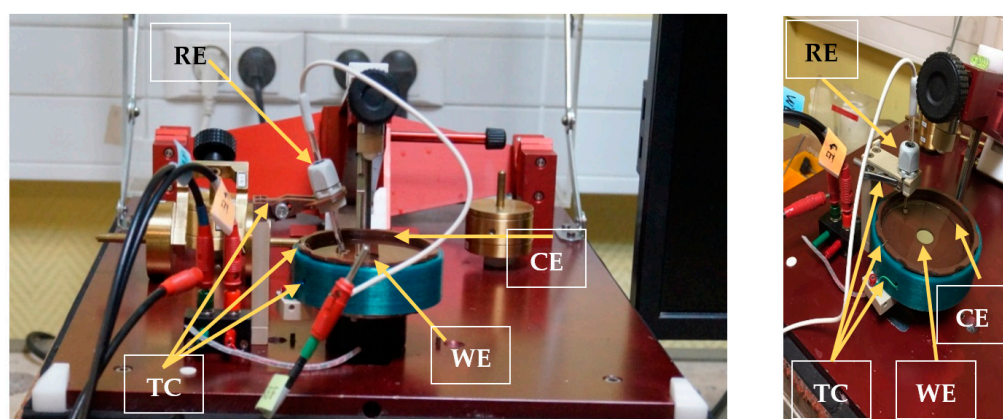


**Figure 1.** Tribocorrosion tests setup: in-house-designed and built tribocorrosion cell (TC), reference electrode (RE), counter electrode (CE) Pt coil, working electrode (WE), and electrical connections to potentiostat.

As indicated before, the electrolyte used was an aqueous 3.5%wt NaCl aerated solution, whose volume was maintained constant (35 mL) for all the experiments. The electrochemical characterization, involved the determination of potentiodynamic polarization curves, which were obtained by following the usual standard procedure. Firstly,

the specimens were immersed in the aqueous solution and monitored for 15 min, to establish the open circuit potential (OCP) and free corrosion conditions prior to starting the tribocorrosion tests. Subsequently, the potentiodynamic polarization curves were obtained, starting from the cathodic branch up to the anodic branch, from  $-400$  mV to about  $+800$  mV, at a scan rate of  $0.5$  mVs $^{-1}$ . The corrosion measurements were performed using a potentiostat/galvanostat Solartron 1287 (Ametek, Berwyn, PA, USA). During the tribocorrosion tests, the potential ( $E$ ), current ( $I$ ), and coefficient of friction (CoF) were recorded simultaneously.

### 2.3.3. Wear Track Characterization

Wear-corrosion volume losses were estimated from optical profilometry measurements of the wear tracks, performed at four different locations, equally spaced along their perimeter. An average cross-section area ( $A$ ) was obtained from the measured profiles and then multiplied by the nominal wear track perimeter (2 mm radius), to estimate the volume loss and wear rate. The wear tracks were analyzed by using a Veeco NT-9300 (Brucker, Billerica, MA, USA) optical profilometer. Thus, 3D measurements of the surface topography (on an approx.  $2 \times 1.5$  mm $^2$  surface) were obtained, which allowed the evaluation of the tribocorrosion performance of the MWCNTs-reinforced WC-Co coating cermets. In addition, SEM techniques (S-520 Hitachi microscope, Tokyo, Japan) were employed for the analysis of the wear track morphology of the coated samples and the identification of the wear mechanisms.

## 3. Results and Discussion

### 3.1. Feedstock Powder and Microstructure Characterization

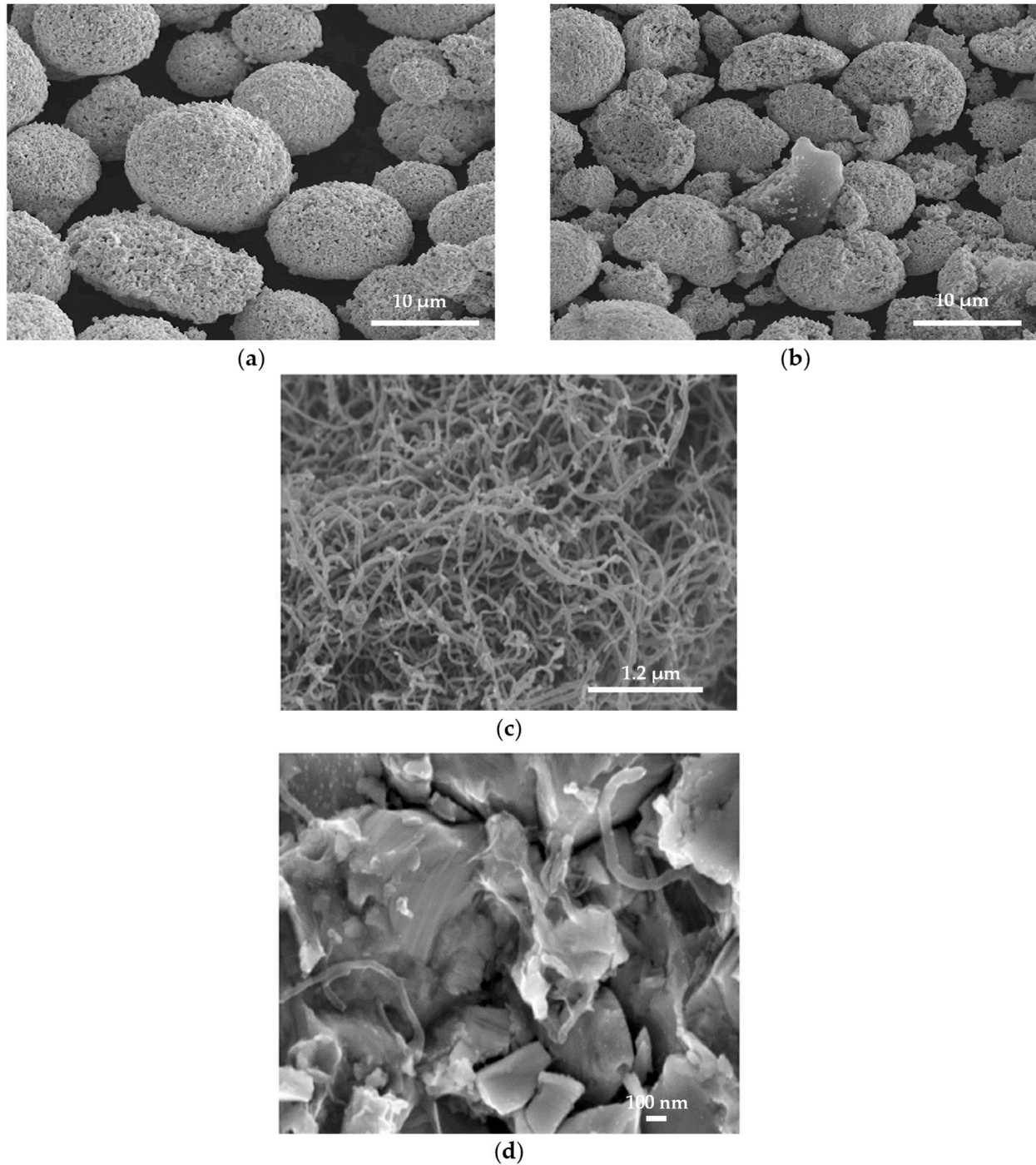
The morphologies of the feedstock powders and MWCNTs used in this research, are shown in Figure 2. The particle size of the as-received WC-12Co powder (Figure 2a), P-WC<sub>AS-RECEIVED</sub>, varies from a few micrometers to no more than 20  $\mu$ m, with a roughly spherical shape. As expected, after the 36 h milling process, the conventional WC-12Co powder particles (Figure 2b), P-WC<sub>CONV</sub>, are noticed by their greater heterogeneity in terms of particle size distribution, which is expected to influence the quality of the HVOF-sprayed coatings and the decarburization process [16].

It has been previously reported that MWCNTs increase the powder particles' bonding strength [16,19]. In fact, MWCNTs tend to form bridges between milled powder particles, which at this stage have a favorable surface matrix to keep the bonds with the MWCNTs.

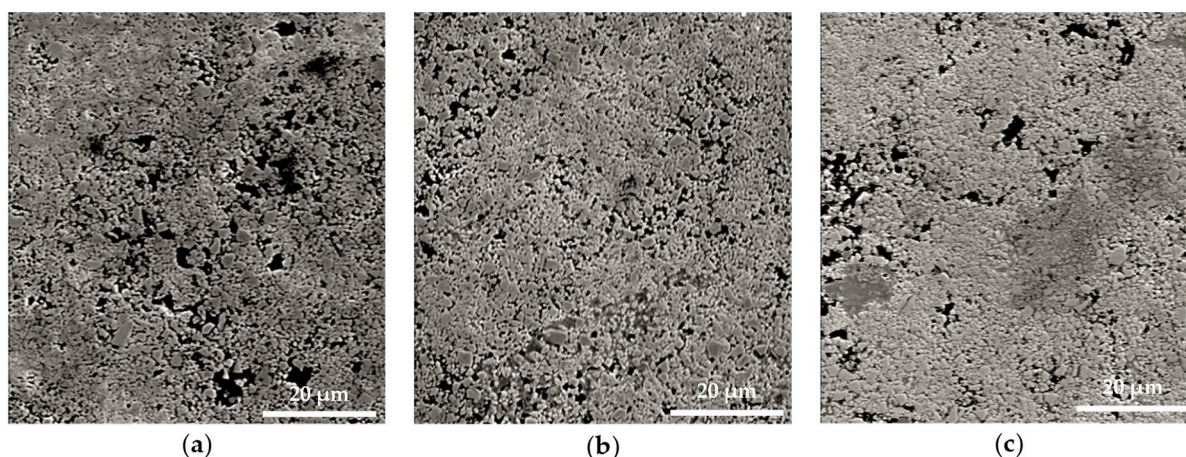
The investigations of Zeng et al. [19], on the dispersion of MWCNTs within the matrix of Mg–Al alloys, led to the conclusion that ball milling of MWCNTs mixtures not only improved their dispersion within the Mg alloy matrix, but also activated their surfaces, increasing their compatibility within the Mg alloy matrix and melt. Consequently, the holding of the MWCNTs in a suspension within the Mg alloy melt was enhanced, and their binding force within the matrix increased. Furthermore, it has been reported that milling processes are responsible for improving, not only the dispersion within the metal matrix, but also for unpacking MWCNTs agglomerates, promoting the enhancement of the binding force of MWCNTs with the matrix and their suitable adhesion to WC-Co particles [16].

Figure 3 shows SEM micrographs, in secondary electrons mode, of the polished cross-section of the HVOF-sprayed coating samples, deposited from WC–Co feeding powders. The thickness and porosity of each coating is reported in Table 1. Accordingly, HVOF-sprayed coating WC<sub>AS-RECEIVED</sub> (P-WC<sub>AS-RECEIVED</sub> feedstock powder not subjected to milling) achieved a thickness of  $453 \pm 5$   $\mu$ m, whereas the WC<sub>CONV</sub> coating (36 h milled conventional feedstock powder, P-WC<sub>CONV</sub>) and the WC<sub>CNT</sub> coating (36 h milled MWCNTs-reinforced conventional feedstock powder, P-WC<sub>CNT</sub>) achieved thicknesses of  $540 \pm 5$   $\mu$ m and  $520 \pm 6$   $\mu$ m, respectively. The examination of the above micrographs allows an evaluation of the porosity of the different samples. Thus, the coatings identified as WC<sub>AS-RECEIVED</sub> (Figure 3a), WC<sub>CONV</sub> (Figure 3b), and WC<sub>CNT</sub> (Figure 3c) were observed to have porosities of  $\sim 3.3 \pm 0.4\%$ ,  $2.3 \pm 0.3\%$ , and  $1.3 \pm 0.3\%$ , respectively. It is worth highlighting the

effect of the milling process on the decrease in the coating porosity, which can be clearly observed by comparing the  $WC_{AS-RECEIVED}$  coating (not milled feedstock) with the other two ( $WC_{CONV}$  and  $WC_{CNT}$  coatings subjected to the milling process), in agreement with the results reported elsewhere [17,18].



**Figure 2.** SEM micrographs of the WC-12Co feeding powders and MWCNTs: (a) P- $WC_{AS-RECEIVED}$ , (b) P- $WC_{CONV}$ , and (c) MWCNTs, and (d) 36 h milling blended P- $WC_{CNT}$ .



**Figure 3.** SEM images (in SE mode) of coatings: (a)  $WC_{AS-RECEIVED}$ , (b)  $WC_{CONV}$ , and (c)  $WC_{CNT}$ .

### 3.2. Tribocorrosion Performance

The tribocorrosion performance of the WC-12Co HVOF-sprayed coatings was evaluated in terms of electrochemical measurements and coefficients of friction, determined from wear tests under potentiodynamic polarization conditions (from  $-400$  mV to about  $+800$  mV vs OCP), as well as from wear-corrosion volume losses. As explained in Section 2.3.2., before wear took place, the three samples were monitored for 15 min, to establish correctly the free-corrosion condition, i.e., the OCP.

#### 3.2.1. Electrochemical Measurements

As indicated above, the tribocorrosion behavior of the WC-12Co HVOF-sprayed samples, in terms of electrochemical response, was assessed by means of potentiodynamic polarization tests, in an aqueous 3.5% NaCl electrolyte. The potentiodynamic polarization curves of the three samples are shown in Figure 4. From this figure, it is noticed that the curves show a small offset from each other. Nevertheless, electrochemical corrosion data obtained from the potentiodynamic polarization tests exhibit slight differences regarding the corrosion properties of the different HVOF-sprayed coatings, which are worth discuss.

For instance, Figure 4 shows minor differences between the corrosion potential ( $E_{corr}$ ) of the different samples, which is observed to vary from  $-350$  to  $-380$  mV. Nevertheless, the corrosion current density ( $i_{corr}$ ) is quite different. The  $WC_{AS-RECEIVED}$  coating (conventional powder not subjected to milling process) shows the lowest  $i_{corr}$ , around  $1.50 \times 10^{-5}$  mA/cm<sup>2</sup>, whereas the  $WC_{CONV}$  coating (36 h milled conventional powder as feedstock) exhibits an increase of  $\sim 15\%$  in the corrosion current density, as compared with the first one.

On the contrary, the  $WC_{CNT}$  coatings (36 h milled MWCNTs-reinforced conventional powder as feedstock) exhibit a remarkable increase in  $i_{corr}$ , representing almost 3 times the one computed for  $WC_{AS-RECEIVED}$  coatings. This significant difference between the corrosion current density of the samples can be associated with the prevailing corrosion mechanisms. On the one hand, the contribution of crevice corrosion will be increased as the porosity of the coatings increases, acting as a concentration of micro-cells. On the other hand, the influence of galvanic corrosion on the electrochemical process (micro-galvanic couple) will be affected by the difference between the electrochemical potential and the composition of the microstructural phases present in the coatings (where the binder phase behaves as anode and WC acts as cathode).

The competition between these two mechanisms is expected to influence the value of  $i_{corr}$  of the system and the corrosion products, comprised mainly of oxides ( $MO_x$ ) and hydroxides  $M(OH)_x$ . These results highlight the complexity of the electrochemical processes, which depend not only on the composition of the existing phases, but also on the coating's microstructure, surface porosity, and topography. Concerning the anodic branch of the polarization curves (Figure 4), it is interesting to observe that the passivation range of

this type of coating [20] cannot be detected under tribocorrosion conditions, possibly due to the continuous sliding process, which hinders the re-passivation ability of these materials.

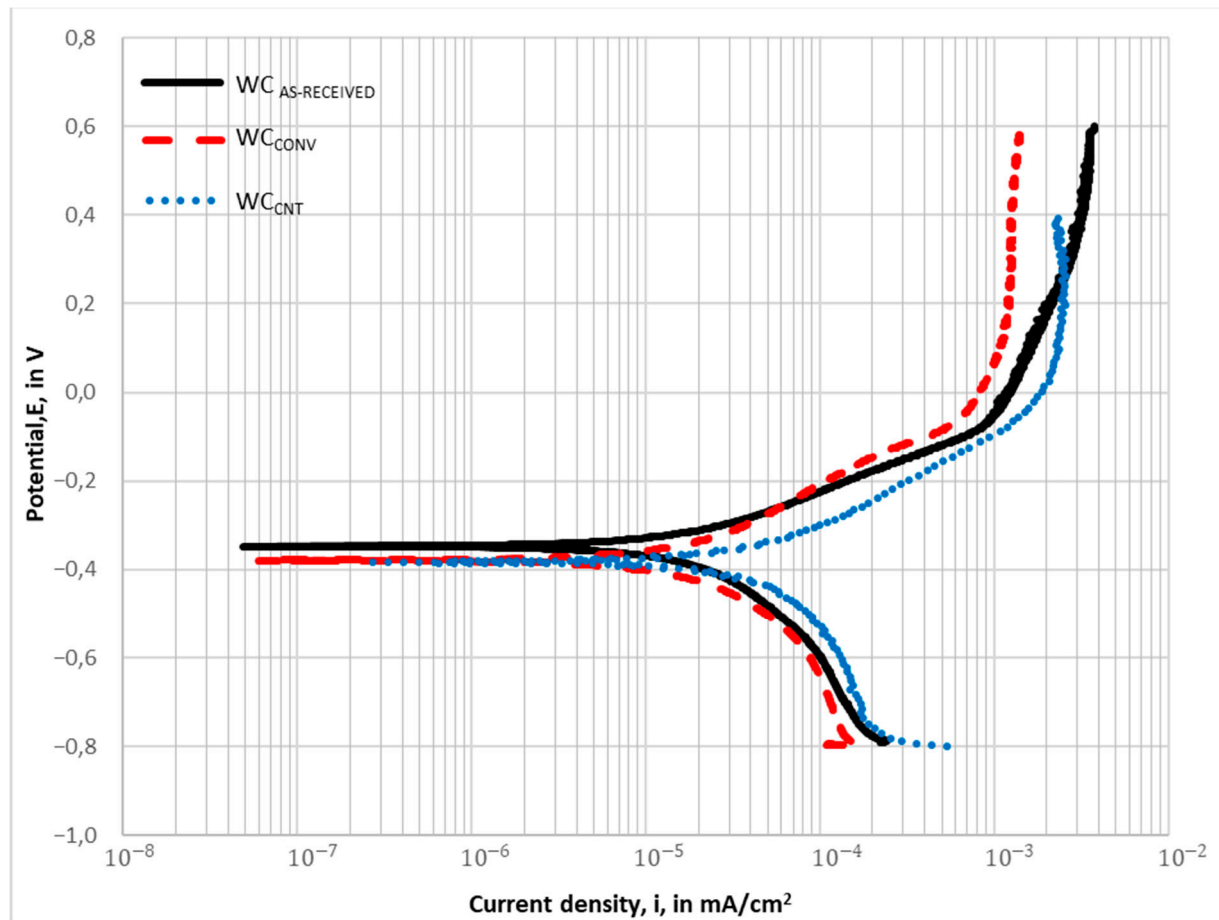


**Figure 4.** Dynamic polarization curves for the HVOF WC-Co system coatings.

Table 2 presents the possible phases which exist in the coatings depending on the feedstock processing. Previous works [20,21] have indicated the presence of  $W_2C$  and  $W$  associated with the decarburization process, related to the nucleation of nanometric phases promoted by the fast-cooling rate of the coating during spraying or by subsequent heat treatments [20]. This decarburizing process, which occurs during deposition, produces  $W$  carbides surrounded by a  $W$ -free cobalt matrix, amorphous phases,  $\eta$  phase ( $Co_3W_3C$ ), and  $W_2C$ , as revealed by XRD analysis, as reported elsewhere [21].

**Table 2.** Electrochemical corrosion data from tribocorrosion tests of WC-12Co HVOF-sprayed coatings.

Sample	$E_{corr}$ (mV)	$i_{corr}$ ( $10^{-5}$ mA/cm <sup>2</sup> )	Median Particle Powder Size ( $\mu$ m)	Possible Phases
WC <sub>AS-RECEIVED</sub>	−350	$1.50 \pm 0.13$	28	WC, $W_2C$ , and MWCNTs
WC <sub>CONV</sub>	−370	$1.64 \pm 0.10$	18	WC, $W_2C$ , $W$ , and $Co_3W_3C$
WC <sub>CNT</sub>	−380	$4.30 \pm 0.20$	18	WC, $W_2C$ , $W$ , $Co_3W_3C$ , and MWCNTs

### 3.2.2. Evaluation of the Coefficient of Friction (CoF)

The friction coefficient associated with the deposited thermal sprayed coatings was evaluated under tribocorrosion conditions and measured from the beginning of the sliding contact, just after the OCP was stabilized. Figure 5 illustrates the behavior of the CoF for the three samples, which exhibits a run-in period of around 800 cycles for all of them.

In addition, it can be observed that the CoF of each of the three samples has a similar fluctuation amplitude, with values in the range of 0.12 to 0.21.

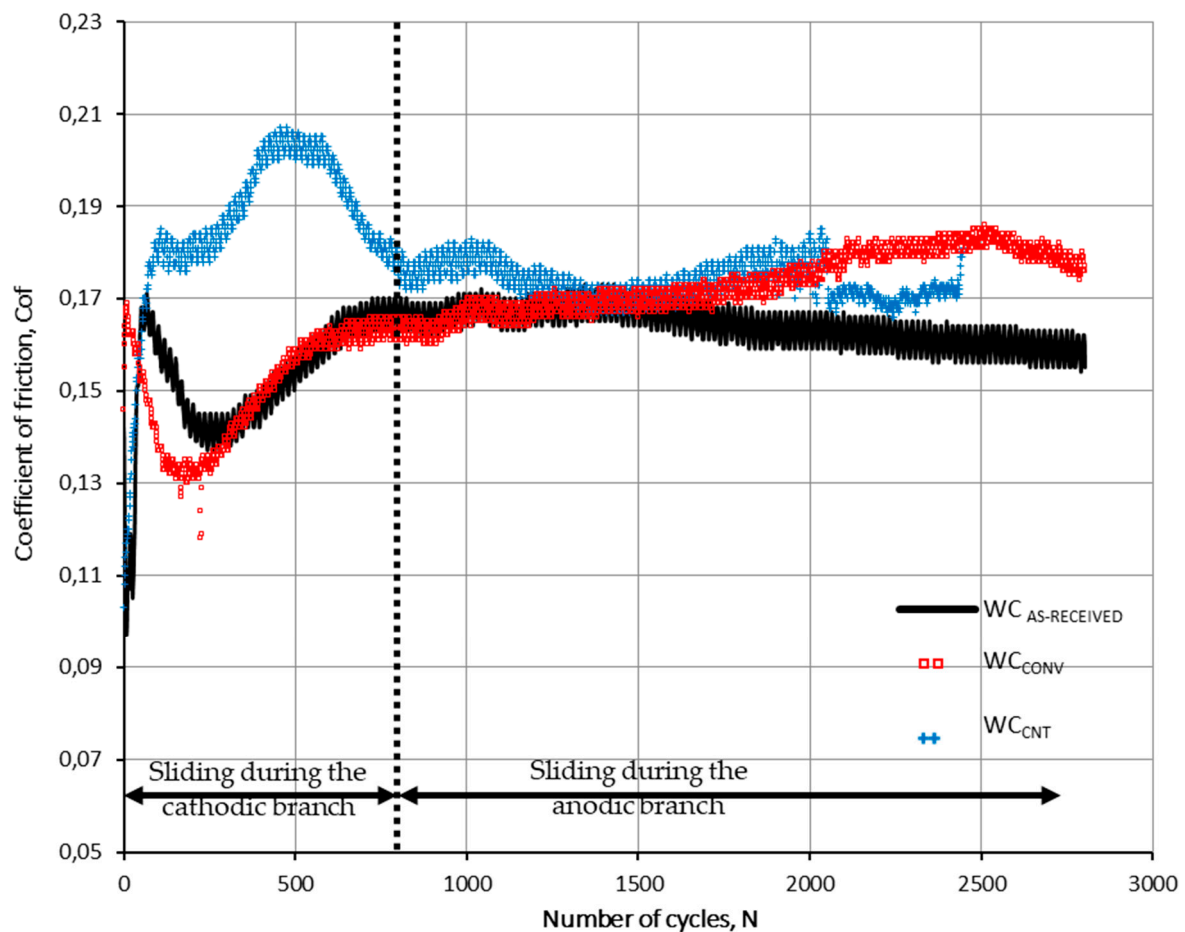


**Figure 5.** Coefficient of friction (CoF) as a function of number of cycles for the HVOF-sprayed coatings, at a load of 10 N, against a 10 mm  $\text{Al}_2\text{O}_3$  ball as counterpart. The sliding distance was set at 35 m, at a rotational speed of 60 rpm and a nominal wear track radius of 2 mm.

For the WC-12Co coatings, the tribocorrosion processes can be divided into three stages as follows: before 100 cycles (initial stage), the coefficients of friction of the three coatings are almost superimposed, primarily due to their similar surface topography and surface roughness. In the range of 100 to 800 cycles (intermediate stage), in the cathodic branch of the polarization curves, the  $\text{WC}_{\text{CONV}}$  and  $\text{WC}_{\text{AS-RECEIVED}}$  coatings exhibit a run-in period where the CoF varies from 0.12 to 0.17, whereas for the  $\text{WC}_{\text{CNT}}$ , it changes between 0.17 and 0.21. After 800 cycles (stable stage) up to approximately 1600 cycles, the CoF of the three coatings shows relatively low variations with respect to the number of cycles, and remains approximately constant, at a value close to 0.18.

The wear track profiles were optically analyzed by means of 2D and 3D imaging, employing optical profilometry, as shown in Figure 6, which allowed the observation of a surface topography typical of a mechanical contact between the  $\text{Al}_2\text{O}_3$ -ball and the coated samples. From these 3D topographic images (Figure 6a,c,e), the damage mechanism observed on all samples was seen to be abrasive wear. The topography difference between the wear track and the reference surface allowed the estimation of the wear volume loss, by means of optical profilometry, as described in the next section. On the other hand, in the 2D optical profilometry images (Figure 6b,d,f), it can be observed that the wear damage on the  $\text{WC}_{\text{CONV}}$  coating is apparently less (thinner wear track) than that of the  $\text{WC}_{\text{AS-RECEIVED}}$  and  $\text{WC}_{\text{CNT}}$  coatings. In particular, the wider wear track on the  $\text{WC}_{\text{CNT}}$  could be explained

by the fact that the chemical damage (higher corrosion current density) induced by the synergy between the prevailing corrosion mechanisms (concentration micro-cells and micro-galvanic couple), accelerates the material loss. This observation was corroborated by the wear volume computation, which is also presented in the next section.

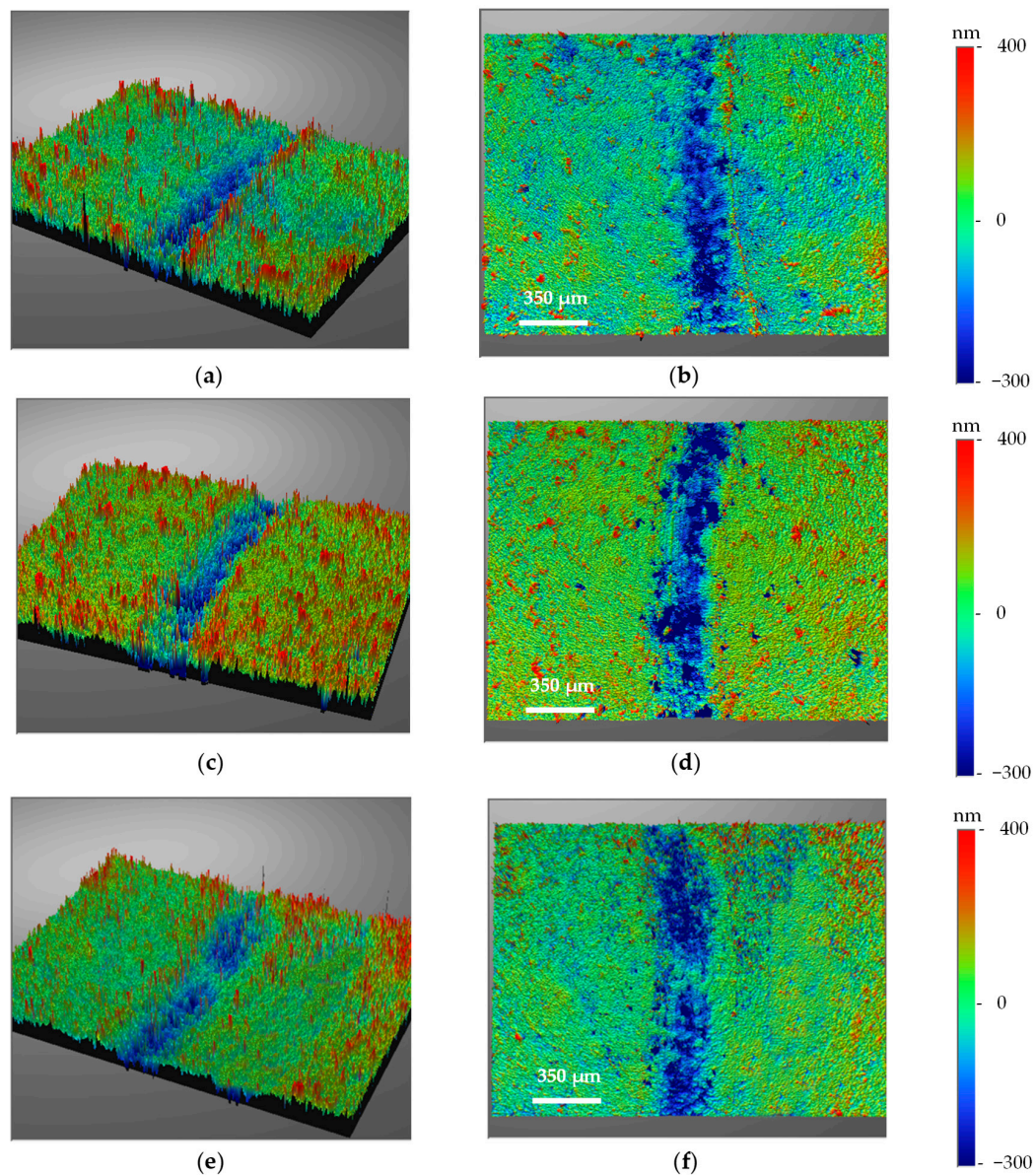


**Figure 6.** Optical analysis (3D and 2D optical profilometry images, respectively) of WC-sprayed coating samples after tribocorrosion tests: (a,b)  $WC_{AS-RECEIVED}$ , (c,d)  $WC_{CONV}$ , and (e,f)  $WC_{CNT}$ .

SEM images of the wear tracks are presented in Figure 7. The presence of scratches indicate that abrasion is the prevailing damage mechanism of the investigated samples, with an insignificant contribution from adhesive damage and plastic deformation. The analysis indicates that abrasion damage could be intimately associated with the detachment of the WC particles, as shown in Figure 7a,e,f, corresponding to the  $WC_{AS-RECEIVED}$ ,  $WC_{CONV}$ , and  $WC_{CNT}$ , respectively. As has been reported elsewhere [9], the detachment of the WC particles is due to the weakening of the WC/binder interfaces in the corrosion environment, which provides straightforward pathways for the nucleation and growth of lateral and vertical cracks produced by the mechanical contact.

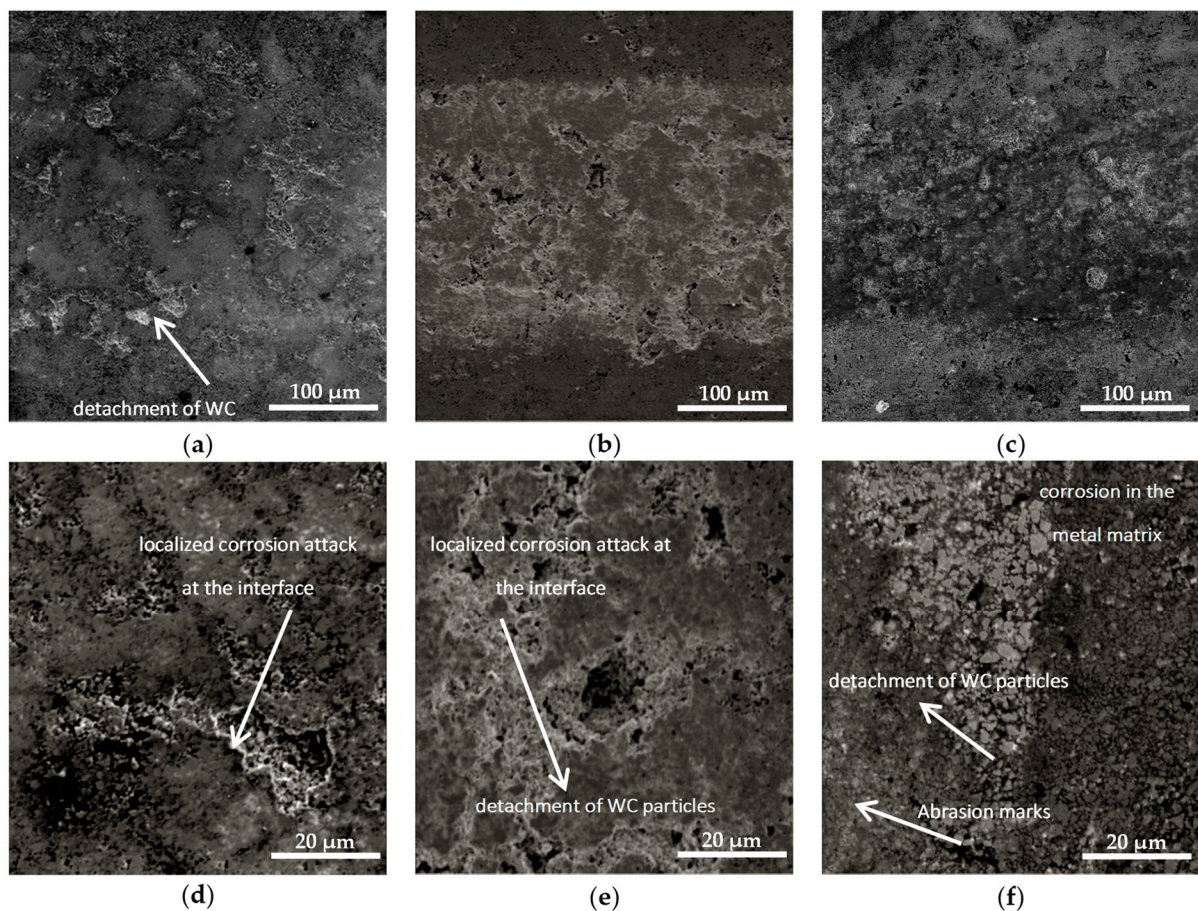


**Figure 7.** SEM images of the different coatings showing chemical and mechanical phenomena on the samples wear track after tribocorrosion testing: (a)  $WC_{AS-RECEIVED}$ , (b)  $WC_{CONV}$  and (c)  $WC_{CNT}$  at 300X magnification; (d)  $WC_{AS-RECEIVED}$ , (e)  $WC_{CONV}$  at and (f)  $WC_{CNT}$  at 1500X magnification.

The sliding contact between the hard counterpart and the coated samples also gives rise to considerable cracking at the coating's surface, as well as the elimination of the wear-corrosion products from the track, which contributes to the formation of third-body particles. Therefore, depending on the solubility of these particles into the electrolyte solution, the removal of the deposited coatings could be accelerated.

From the SEM analysis of the  $WC_{CNT}$  coating sample, significant differences in the morphological aspects, associated with the chemical phenomena occurring inside (Figure 7f) and outside (Figure 8), of the wear track can be observed. Figure 8 indicates that, outside the wear track, the corrosion products probably correspond to a mixture of CoO (or  $Co(OH)_2$ ) and  $WO_3$ , as has also been reported in previous research works [22–24]. The formation of cobalt oxide (CoO) has been reported to be responsible for a primary passivity potential region in neutral and basic solutions [22].

On the other hand, the hydroxide  $Co(OH)_2$  is known to be slightly soluble in NaOH and KOH solutions. This hydroxide is more likely to be the first film formed rather than the oxide, and its dissolution will contribute to the values corresponding to the anodic or cathodic currents [24]. Chen et al. [23] reported that one of the possible reactions, from a thermodynamic point of view, could give rise to the presence of  $WO_3$ . Given the significant presence of corrosion products inside the wear track, as well as abrasion marks produced by the contact against the  $Al_2O_3$  ball counterpart, it is expected that the applied contact pressure also plays an important role in the removal of the  $Co(OH)_2$  film, exposing the CoO in the metal matrix, as observed in Figure 7f.

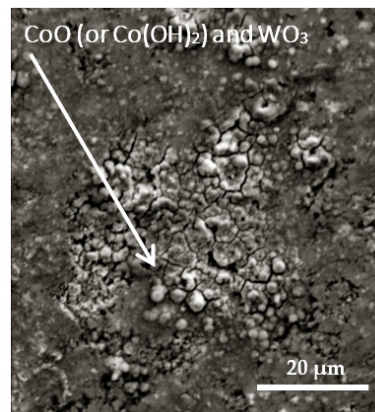


**Figure 8.** SEM image of corrosion products outside of the wear track of the WC<sub>CNT</sub> coating after tribocorrosion tests.

Under tribocorrosion conditions, the WC-12Co HVOF-sprayed coatings undergo an increase in the abrasion effect, as compared to tests without any anodic condition, due to the low corrosion resistance of the metal matrix. Testing conditions corresponding to the anodic branch of the potentiodynamic polarization curve (Figure 4) enhance the corrosion process of the cobalt matrix, and therefore WC particles can easily be detached from the matrix, inducing an increase in abrasion damage and volume loss, as has been previously reported [20]. This carbide removal, intensified by the matrix dissolution, is the principal damage mechanism that operates during the tribocorrosion testing.

It is worth noting that the WC<sub>CNT</sub> coating exhibited the highest evidence of abrasion damage in the wear track. This can be explained by the fact that carbide fragments are detached from the cobalt matrix due to the action of the shear forces, which arise from the sliding contact of the counterpart on the samples surface. Once the carbides are fragmented, these forces can be transmitted into the metal matrix, giving rise to its cracking, as well as that of the ceramic phase. Such a cracking promotes the detachment of MWCNTs from the matrix and increases the free reactive surface of the coated sample.

The growth of a reactive surface under tribocorrosion conditions, when anodic polarization takes place, has also been previously reported elsewhere [20]. Moreover, it has been acknowledged that, due to the different values of the expansion coefficient, after deposition the cobalt-rich binder phase remains under tension, whereas the WC phase is in a state of compression. Thus, the inherent residual stress difference intrinsic to the coating production will allow the nucleation and propagation of cracks, which will increase due to the mechanical contact between the Al<sub>2</sub>O<sub>3</sub>-ball and the sample, contributing in this way to the decrease in the tribocorrosion resistance [25].

The hardness and fracture toughness of the WC<sub>CONV</sub> and WC<sub>CNT</sub> coatings have been evaluated and reported elsewhere [18]. According to the authors, the fracture toughness of the WC<sub>CNT</sub> coatings, of  $\sim 5.4 \pm 0.2 \text{ MPa}\cdot\text{m}^{1/2}$ , is somewhat greater than that of the WC<sub>CONV</sub> coatings, of  $\sim 4.3 \pm 0.3 \text{ MPa}\cdot\text{m}^{1/2}$ . The results of the present investigation corroborate this, demonstrating that such an increase in fracture toughness of the WC<sub>CNT</sub> coating, as compared to the WC<sub>CONV</sub> one, is due not only to a remarkable decrease in porosity, but also to the increase in the bond strength between the lamellae and MWCNTs, as has been previously reported [18]. Nevertheless, when the WC<sub>CNT</sub> coating is subjected to tribocorrosion conditions, both the fragmented carbides, detached from the cobalt matrix, and the low corrosion resistance of the metal matrix, would give rise to an apparent decrease in the fracture toughness, which would explain the reported results. Therefore, as described elsewhere [20], the tribocorrosion resistance would be expected to decrease due to decohesion of the phases and free reactive surface growth.

It has been shown in [18] that reinforcement by MWCNTs increased the wear resistance, by forming inter-splat bridges and acting as a lubricant, whereas the improvement in the hardness was attributed to their deformation resistance. Additionally, it has been

determined that the fracture toughness increased for the  $WC_{CNT}$  coating, as compared to the  $WC_{CONV}$  coating, by approximately 30%, which also explained the improvement in the wear resistance of the reinforced material. Therefore, the  $H^3/(E^*)^2$  ratio should be considered, since it is a measure of the resistance to plastic deformation of the coating. In the above ratio,  $H$  represents the hardness and  $E^*$  the plain strain elastic modulus. In our case, taking into consideration that the addition of MWCNTs did not give rise to any significant change in the elastic modulus, the hardness alone can be used as a reference parameter for anticipating the wear behavior.

The phenomenon usually referred to as “telescopic effect” [26], where the inner tubes of MWCNTs are susceptible to being pulled-out of the outer tube by tensile stresses, was not expected to occur in these reinforced coatings, since there is a random orientation distribution of the MWCNTs, which minimizes this effect.

The present investigation has also allowed the corroboration of previous results concerning the absence of a passivity range in cermet coatings when subjected to any external loads [20,27]. Accordingly, the passivity range in WC-Co coatings have been reported to be related to the formation of a thin layer composed of  $WO_3$  and  $CoO$ , which hinders Co dissolution under anodic corrosion conditions [28,29]. However, continuous abrasion is expected to remove this layer, giving rise to its de-passivation and Co dissolution. The passivation rate of WC-Co coatings has been reported to be directly proportional to the thickness of the WC layer formed [29]. Tribocorrosion conditions impede the re-passivation of the coatings, due to the removal of the thin oxide protective film, which grows between sliding cycles.

The present results indicate that the presence of MWCNTs in addition to WC, will slightly enhance the dissolution of the Co matrix, due to the galvanic couple that is formed between the matrix and the mixture of WC and MWCNTs. Thus, the selective dissolution of the matrix would give rise to the presence of a somewhat greater quantity of isolated constituents. Therefore, the addition of MWCNTs is not likely to improve the corrosion behavior of these coatings.

The  $Al_2O_3$  counterparts did not exhibit any remarkable damage on their surfaces after tribocorrosion testing. Neither debris accumulation nor significant scratch abrasion marks were observed on their surfaces. As expected, debris adhesion to the counterparts was not observed, due to the high melting temperature of the existing phases at the sliding contact (WC, Co, MWCNTs,  $Al_2O_3$ ) and the low temperatures reached during the tribocorrosion tests.

### 3.2.3. Wear Constant Computation

The volume loss ( $V$ ) of the coatings was computed according to the ASTM G99 standard:

$$V = 2\pi rA \quad (1)$$

where  $r$  is the nominal radius, and  $A$  is the cross-sectional area of the wear track, determined from optical profilometry measurements. The wear constant ( $K$ ) was obtained by means of the Archard equation [30], expressed as follows:

$$K = \frac{V}{P \cdot l} \quad (2)$$

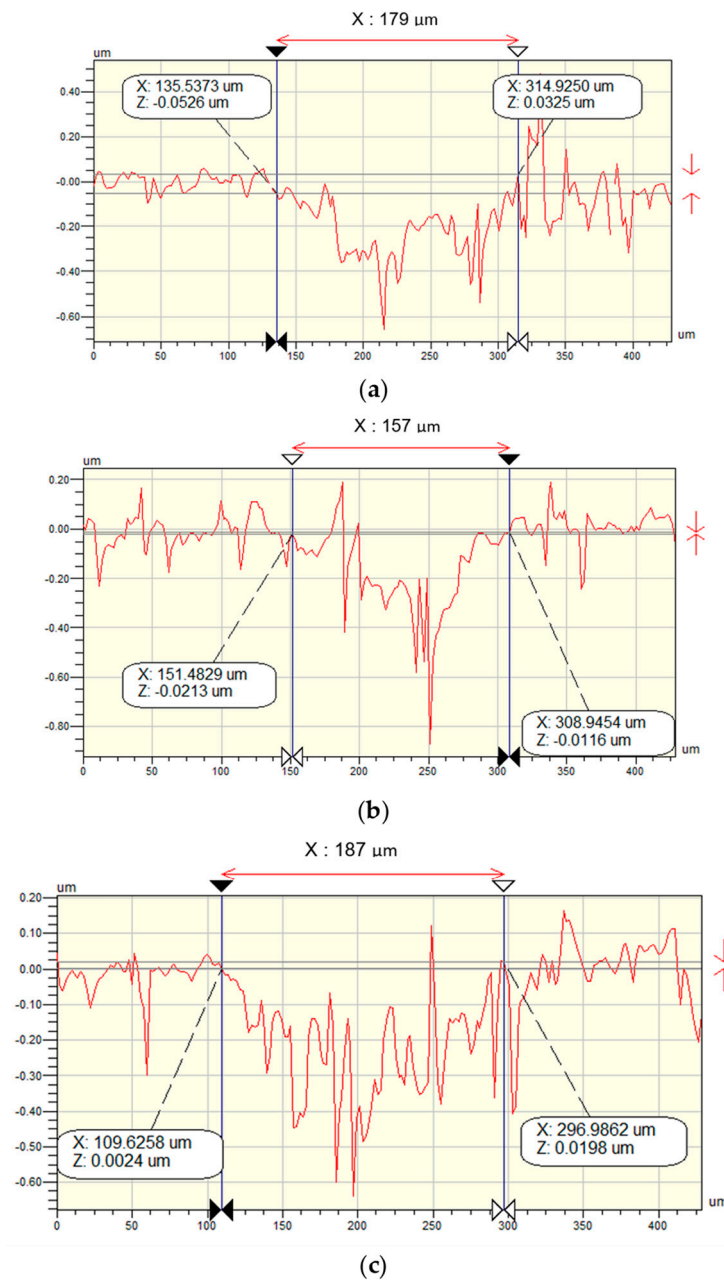
where  $P$  is the applied normal load, and  $l$  the sliding distance for each tribocorrosion test.

Table 3 presents the values of the volume loss and wear coefficient determined for the different samples, tested under the tribocorrosion conditions.

**Table 3.** Computed volume loss ( $V$ ) and wear constant ( $K$ ) obtained from the tribocorrosion tests of the WC-12Co HVOF-sprayed coatings.

Sample	Volume Loss, $V$ ( $\text{mm}^3$ )	Wear Constant, $K$ ( $10^{-12} \text{ m}^3/\text{Nm}$ )
WC <sub>AS-RECEIVED</sub>	$0.55 \pm 0.02$	$1.5 \pm 0.05$
WC <sub>CONV</sub>	$0.53 \pm 0.03$	$1.5 \pm 0.08$
WC <sub>CNT</sub>	$0.63 \pm 0.04$	$1.8 \pm 0.1$

The wear track profiles of the tested samples were analyzed by means of optical profilometry and are shown in Figure 9.



**Figure 9.** Wear track profiles obtained by means of optical profilometry of the HVOF-sprayed coating samples after tribocorrosion testing: (a) WC<sub>AS-RECEIVED</sub>, (b) WC<sub>CONV</sub>, and (c) WC<sub>CNT</sub>.

The WC<sub>AS-RECEIVED</sub> and WC<sub>CONV</sub> coated samples showed a very small difference in their behavior, which was corroborated by the similar estimated volume losses, as reported

in Table 3 ( $WC_{AS-RECEIVED}$ :  $0.55 \pm 0.02 \text{ mm}^3$ , and  $WC_{CONV}$ :  $0.53 \pm 0.03 \text{ mm}^3$ ). Nonetheless, a remarkable difference between the 36 h milled conventional powder mixed with the MWCNTs feedstock ( $WC_{CNT}$ ), and the other two coatings ( $WC_{AS-RECEIVED}$  and  $WC_{CONV}$ ), can be observed. The  $WC_{CNT}$  coating volume loss was estimated to be  $0.63 \pm 0.04 \text{ mm}^3$ . This result suggests that the  $WC_{CNT}$  coating surface (even showing the lowest porosity) exhibits less tribocorrosion resistance as compared with the  $WC_{AS-RECEIVED}$  and  $WC_{CONV}$  coatings. Consequently, a higher quantity of debris and Co dissolution is produced.

Besides the volume loss, the current density,  $i_{corr}$ , of the  $WC_{CNT}$  coating was calculated to be 2.6 times the  $i_{corr}$  value of the  $WC_{CONV}$  coating and 2.9 times the value corresponding to the  $WC_{AS-RECEIVED}$  coating, as reported in Table 2. In addition, it has been shown that under tribocorrosion conditions the addition of MWCNTs does not provide any improvement in the coefficient of friction, which remains around the same value for all WC-12Co HVOF-sprayed coated samples, in agreement with previous research works [17,31–33].

Tables 2 and 3 summarize the electrochemical data ( $E_{corr}$  and  $i_{corr}$ ) and volume loss from tribocorrosion tests conducted under the same conditions (wear sliding under potentiodynamic polarization scan from  $-400 \text{ mV}$  to about  $+800 \text{ mV}$ ), for each WC-12Co HVOF-sprayed coating. From these tables, it is worth noting that the milling process ( $WC_{CONV}$  and  $WC_{CNT}$ ) does not give rise to an improvement of the corrosion potential of these coatings, as compared with that produced by employing the feedstock powder ( $WC_{AS-RECEIVED}$ ). The corrosion potential ( $E_{corr}$ ) varies from  $-350 \text{ mV}$  in the  $WC_{AS-RECEIVED}$  coated sample, to  $-370 \text{ mV}$  in the  $WC_{CONV}$  coated specimen, and undergoes a shift of approximately 8% ( $-380 \text{ mV}$ ) in the case of the  $WC_{CNT}$  coating. Thus, the porosity is not the only parameter playing a significant role in the corrosion mechanisms of the coatings.

The coupling effect between wear and corrosion has a marked influence on the  $WC_{CNT}$  coating regarding the increase in the current density (almost 3 times higher than  $WC_{AS-RECEIVED}$  coating), the decrease in the corrosion potential (around 8% less than the  $WC_{AS-RECEIVED}$  coating), and the increase in the volume loss and wear constant (about 20% higher than the  $WC_{AS-RECEIVED}$  coating), when the coating is subjected to wear under a potentiodynamic scan. This illustrates the complex mechanisms prevailing under tribocorrosion conditions, which give rise to concurrent interacting phenomena, involving both electrochemical and mechanical responses.

Concerning the evolution of the coefficient of friction during the whole test for each sample, slight differences were observed between the coatings. These results could suggest that under tribocorrosion conditions the addition of MWCNTs does not significantly improve the contact between the counterpart and the WC-12Co HVOF-sprayed coatings, contrary to the improvement that has been reported under dry wear testing conditions [17]. Nevertheless, the NaCl electrolyte acted as a lubricant, having the same tribological effect on the three samples, as confirmed by the similar values of this parameter obtained under steady state conditions, which for all of them was approximately 0.18.

#### 4. Conclusions

The tribocorrosion performance of MWCNTs-reinforced WC-12Co HVOF-sprayed cermet coatings was successfully characterized, and the following conclusions can be drawn based on the results and discussions presented in this research work:

- The reinforced  $WC_{CNT}$  coating exhibited an increase in the corrosion current density of approximately 3 times, as compared with both the  $WC_{AS-RECEIVED}$  and  $WC_{CONV}$  coatings. The formation and removal of multi-oxide films of CoO (or  $\text{Co}(\text{OH})_2$ ) and  $\text{WO}_3$ , under aqueous conditions, control the coating's performance during the mechanical contact under electrochemical conditions (potentiodynamic scan).
- The NaCl electrolyte acts as a lubricant and an average friction coefficient value of 0.18 is attained once the system achieves nearly a steady state regime. Under anodic corrosion conditions, MWCNTs reinforcing does not reduce the coefficient of friction between the counterpart and the WC-12Co HVOF-sprayed coatings.

- Wear appears to occur by carbide ejection due to a selective dissolution of the matrix during the tribochemical process.
- The wear constants are of the same order of magnitude ( $\sim 10^{-12}$  m<sup>3</sup>/Nm). Nevertheless, the reinforced WC<sub>CNT</sub> coating exhibits a higher current density (approximately 3 times), a higher wear rate (about 20%), and a lower corrosion potential (shift 8% down) than the WC<sub>AS-RECEIVED</sub> coating.
- These results provide an approach to discriminate between different coatings' performances under tribocorrosion conditions. Thus, tribocorrosion testing can be used as an industrial protocol to compare the performance of coatings subjected to tribo-chemical conditions.
- Finally, the data obtained from MWCNTs-reinforced WC-12Co HVOF-sprayed coatings evaluated under tribocorrosion conditions represent a contribution to the understanding of the tribological properties of these materials, as a function of their microstructure and testing conditions.

**Author Contributions:** Conceptualization, M.H.S.; methodology, M.H.S., A.M. and S.K.; validation, M.H.S., A.M. and S.K.; formal analysis, E.S.P.-C.; investigation, A.M. and S.K.; data curation, A.M. and S.K.; writing—original draft preparation, A.M.; writing—review and editing, M.H.S., A.M. and E.S.P.-C.; visualization, A.M. and M.H.S.; supervision, M.H.S.; project administration, M.H.S. All authors have read and agreed to the published version of the manuscript.

**Funding:** This research received no external funding.

**Institutional Review Board Statement:** Not applicable.

**Informed Consent Statement:** Not applicable.

**Data Availability Statement:** Additional details concerning this work are available from the authors.

**Conflicts of Interest:** The authors declare no conflict of interest.

## References

1. Nouvellon, C.; Belchi, R.; Libralesso, L.; Douhéret, O.; Lazzaroni, R.; Snyders, R.; Thiry, D. WC/C:H films synthesized by a hybrid reactive magnetron sputtering/Plasma Enhanced Chemical Vapor Deposition process: An alternative to Cr(VI) based hard chromium plating. *Thin Solid Film*. **2017**, *630*, 79–85. [[CrossRef](#)]
2. Wang, Q.; Luo, S.; Wang, S.; Wang, H.; Ramachandran, C. Wear, erosion and corrosion resistance of HVOF-sprayed WC and Cr<sub>3</sub>C<sub>2</sub> based coatings for electrolytic hard chrome replacement. *Int. J. Refract. Met. Hard Mater.* **2019**, *81*, 242–252. [[CrossRef](#)]
3. Carneiro, E.; Castro, J.; Marques, S.; Cavaleiro, A.; Carvalho, S. REACH regulation challenge: Development of alternative coatings to hexavalent chromium for minting applications. *Surf. Coat. Technol.* **2021**, *418*, 127271. [[CrossRef](#)]
4. Javed, M.; Ang, A.; Bhadra, C.; Piola, R.; Neil, W.; Berndt, C.; Leigh, M.; Howse, H.; Wade, S. Corrosion and mechanical performance of HVOF WC-based coatings with alloyed nickel binder for use in marine hydraulic applications. *Surf. Coat. Technol.* **2021**, *418*, 127239. [[CrossRef](#)]
5. Vats, A.; Kumar, A.; Patnaik, A.; Meena, M.L. Influence of deposition parameters on Tribological Performance of HVOF Coating: A review. *IOP Conference Series: Mater. Sci. Eng.* **2021**, *1017*, 012015. [[CrossRef](#)]
6. Kumar, H.; Chittosiya, C.; Shukla, V. HVOF Sprayed WC Based Cermet Coating for Mitigation of Cavitation, Erosion & Abrasion in Hydro Turbine Blade. *Mater. Today Proc.* **2018**, *5*, 6413–6420. [[CrossRef](#)]
7. Potgieter, J.H.; Whitefield, D.; Motsumi, V. Electrochemical Corrosion Behaviour of Different Grades of WC-Co, High-Cr White Cast Irons and Hadfield Steel in 1 M Sulphuric Acid. *Materials* **2021**, *14*, 6130. [[CrossRef](#)]
8. Katiyar, P.K. A comprehensive review on synergy effect between corrosion and wear of cemented tungsten carbide tool bits: A mechanistic approach. *Int. J. Refract. Met. Hard Mater.* **2020**, *92*, 105315. [[CrossRef](#)]
9. Boukantar, A.R.; Djerdjare, B.; Guibertau, F.; Ortiz, A.L. A critical comparison of the tribocorrosive performance in highly-alkaline wet medium of ultrafine-grained WC cemented carbides with Co, Co+Ni, or Co+Ni+Cr binders. *Int. J. Refract. Met. Hard Mater.* **2021**, *95*, 105452. [[CrossRef](#)]
10. Bakshi, S.; Lahiri, D.; Agarwal, A. Carbon nanotube reinforced metal matrix composites—A review. *Int. Mater. Rev.* **2010**, *55*, 41–64. [[CrossRef](#)]
11. Deesom, D.; Charoenrut, K.; Moonngam, S.; Banjongprasert, C. Fabrication and properties of NiCr/MWCNTs nanocomposite coatings prepared by High Velocity Oxy-Fuel Spraying. *Surf. Coat. Technol.* **2016**, *306*, 240–244. [[CrossRef](#)]
12. Dong, Y.-R.; Sun, W.-C.; Liu, X.-J.; Jia, Z.-W.; Guo, F.; Ma, M.; Ruan, Y.-Y. Effect of MWCNTs concentration on the microstructure and friction behavior of Ni-GO-MWCNTs composite coatings. *Surf. Coat. Technol.* **2019**, *359*, 141–149. [[CrossRef](#)]

13. Ujah, C.; Popoola, A.; Popoola, O.; Aigbodion, V. Influence of MWCNTs addition on the mechanical, microstructural, and corrosion properties of Al alloy using spark plasma sintering technique. *Int. J. Adv. Manuf. Technol.* **2020**, *106*, 2961–2969. [[CrossRef](#)]
14. Sharma, A.; Das, S.; Das, K. Electrochemical corrosion behavior of CeO<sub>2</sub> nanoparticle reinforced Sn-Ag based lead free nanocomposite solders in 3.5wt.% NaCl bath. *Surf. Coat. Technol.* **2015**, *261*, 235–243. [[CrossRef](#)]
15. Kumar, N.; Sharma, A.; Manoj, M. Influence of Different Aqueous Media on the Corrosion Behavior of B4C-Modified Lightweight Al-Mg-Si Matrix Composites. *Materials* **2022**, *15*, 8531. [[CrossRef](#)] [[PubMed](#)]
16. Rodriguez, M.; Gil, L.; Camero, S.; Fréty, N.; Santana, Y.; Caro, J. Effects of the dispersion time on the microstructure and wear resistance of WC/Co-MWCNTs HVOF sprayed coatings. *Surf. Coat. Technol.* **2014**, *258*, 38–48. [[CrossRef](#)]
17. Santana, Y.; Gutiérrez, M.; Staia, M.; La Barbera-Sosa, J.; Puchi-Cabrera, E.; Iost, A.; Chicot, D. Sliding wear resistance of thermal sprayed wc-12co coatings reinforced with carbon nanotubes. In Proceedings of the Surface Modification Technologies, Mons, Belgium, 5–7 July 2017; Available online: <https://hal.science/hal-03169289> (accessed on 3 June 2022).
18. Staia, M.; Mejias, A.; La Barbera, J.; Puchi-Cabrera, E.; Villalobos-Gutierrez, C.; Santana, Y.; Montagne, A.; Iost, A.; Rodriguez, M. Mechanical properties of WC/Co-CNT HVOF sprayed coatings. *Surf. Eng.* **2020**, *36*, 1156–1164. [[CrossRef](#)]
19. Zeng, X.; Zhou, G.; Xu, Q.; Xiong, Y.; Luo, C.; Wu, J. A new technique for dispersion of carbon nanotube in a metal melt. *Mater. Sci. Eng. A* **2010**, *527*, 5335–5340. [[CrossRef](#)]
20. Valentini, L.; Valente, T.; Casadei, F.; Fedrizzi, L. Mechanical and tribocorrosion properties of HVOF sprayed WC–Co coatings. *Corros. Eng. Sci. Technol.* **2004**, *39*, 301–307. [[CrossRef](#)]
21. De Villiers Lovelock, H. Powder/Processing/Structure Relationships in WC-Co Thermal Spray Coatings: A Review of the Published Literature. *J. Therm. Spray Technol.* **1998**, *7*, 357–373. [[CrossRef](#)]
22. Badawy, W.; Al-Kharafi, F.; Al-Ajm, J. Electrochemical behaviour of cobalt in aqueous solutions of different pH. *J. Appl. Electrochem.* **2000**, *30*, 693–704. [[CrossRef](#)]
23. Chen, W.; Mao, T.; Zhang, B.; Zhang, S.; Meng, X. Designs and preparation of advanced HVOF-PVD duplex coating by combination of HVOF and arc ion plating. *Surf. Coat. Technol.* **2016**, *304*, 125–133. [[CrossRef](#)]
24. Behl, X.; Toni, J. Anodic oxidation of Cobalt in Potassium Hydroxide electrolytes. *Electroanal. Chem. Interfacial Electrochem.* **1971**, *31*, 63–75. [[CrossRef](#)]
25. Zhang, L.; Chen, Y.; Wan, Q.-L.; Liu, T.Z.J.-F.; Tian, W. Electrochemical corrosion behaviors of straight WC–Co alloys: Exclusive variation in grain sizes and aggressive media. *Int. J. Refract. Met. Hard Mater.* **2016**, *57*, 70–77. [[CrossRef](#)]
26. Moghadam, A.D.; Omrani, E.; Menezes, P.L.; Rohatgi, P.K. Mechanical and tribological properties of self-lubricating metal matrix nanocomposites reinforced by carbon nanotubes (CNTs) and graphene—A review. *Compos. Part B Eng.* **2015**, *77*, 402–420. [[CrossRef](#)]
27. Fedrizzi, L.; Rossi, S.; Cristel, R.; Bonora, P. Corrosion and wear behaviour of HVOF cermet coatings used to replace hard chromium. *Electrochim. Acta* **2004**, *17–18*, 2803–2814. [[CrossRef](#)]
28. Lin, J.-C.; Lin, J.-Y.; Jou, S.-P. Selective dissolution of the cobalt binder from scraps of cemented tungsten carbide in acids containing additives. *Hydrometallurgy* **1996**, *43*, 47–61. [[CrossRef](#)]
29. Sun, F.; Chen, X.; Zhao, Z. Anodic passivation on the recycling of cemented carbide scrap by selective electro-dissolution. *Waste Manag.* **2018**, *80*, 285–291. [[CrossRef](#)]
30. Rong Liu, D.L. Modification of Archard's equation by taking account of elastic/pseudoelastic properties of materials. *Wear* **2001**, *251*, 956–964. [[CrossRef](#)]
31. Alishahi, M.; Monirvaghefi, S.; Saatchi, A.; Hosseini, S. The effect of carbon nanotubes on the corrosion and tribological behavior of electroless Ni–P–CNT composite coating. *Appl. Surf. Sci.* **2012**, *258*, 2439–2446. [[CrossRef](#)]
32. Hatipoglu, G.; Kartal, M.; Uysal, M.; Cetinkaya, T.; Akbulut, H. The effect of sliding speed on the wear behavior of pulse electro Co-deposited Ni/MWCNT nanocomposite coatings. *Tribol. Int.* **2016**, *98*, 59–73. [[CrossRef](#)]
33. Soltani, H.; Tavoosi, M.; Loghman-Estarki, M. Fe–Ni composite coatings reinforced with SiC nanoparticles and carbon nanotubes: Corrosion and tribological performance. *Mater. Res. Express* **2019**, *6*, 115106. [[CrossRef](#)]

**Disclaimer/Publisher's Note:** The statements, opinions and data contained in all publications are solely those of the individual author(s) and contributor(s) and not of MDPI and/or the editor(s). MDPI and/or the editor(s) disclaim responsibility for any injury to people or property resulting from any ideas, methods, instructions or products referred to in the content.